

Manganese(II) Oxide Nano-hexapods: Insight into Controlling the Form of Nanocrystals

Teyeb Ould-Ely,[†] Dario Prieto-Centurion,[†] A. Kumar,[†] W. Guo,[‡] William V. Knowles,[§] Subashini Asokan,[§] Michael S. Wong,^{†,§} I. Rusakova,^{||} Andreas Lüttge,^{†,⊥} and Kenton H. Whitmire^{*,†}

Department of Chemistry, MS 60, Center for Biology and Environmental Nanotechnology, Department of Chemical and Biomolecular Engineering, MS362, and Department of Earth Science, MS 126, Rice University, 6100 Main Street, Houston, Texas 77005-1892, and Texas Center for Superconductivity, University of Houston, Houston, Texas 77204-5931

Received November 11, 2005. Revised Manuscript Received January 27, 2006

Cross-shaped and octahedral nanoparticles (hexapods) of MnO in size, and fragments thereof, are created in an amine/carboxylic acid mixture from manganese formate at elevated temperatures in the presence of water. The nanocrosses have dimensions on the order of 100 nm, but with exposure to trace amounts of water during the synthesis process they can be prepared up to about 300 nm in size. Electron microscopy and X-ray diffraction results show that these complex shaped nanoparticles are single crystal face-centered cubic MnO. In the absence of water, the ratio of amine to carboxylic acid determines the nanocrystal size and morphology. Conventionally shaped rhombohedral/square nanocrystals or hexagonal particles can be prepared by simply varying the ratio of tri-*n*-octylamine/oleic acid with sizes on the order of 35–40 nm in the absence of added water. If the metal salt is rigorously dried before the synthesis, then “flower-shaped” morphologies on the order of 50–60 nm across are observed. Conventional square-shaped nanocrystals with clearly discernible thickness fringes that also arise under conditions producing the nanocrosses mimic the morphology of the cross-shaped and octahedral nanocrystals and provide clues to the crystal growth mechanism(s), which agree with predictions of crystal growth theory from rough, negatively curved surfaces. The synthetic methodology appears to be general and promises to provide an entryway into other nanoparticle compositions.

Introduction

The controlled synthesis of nanoparticles has been widely studied in recent years owing to the unusual properties that particles in this size regime display. A large number of potential commercial applications are envisioned for particles having diverse physical and chemical properties, with potential applications ranging from use as magnetic and electronic materials to catalysis and bioremediation. But controlling the growth of nanoparticles under widely divergent conditions is difficult, and most often particles, including noble metals as well as simple chemical compounds, adopt thermodynamically favored forms, including spheres, cubes, hexagons, rods, and nanotubes.^{1–11} More recently, researchers

have developed methods for producing unusual forms such as nanobelts, nanostars, nanotrees, and nanotetrapods.¹ These various forms of nanomaterials show promising applications related to their anisotropic properties.^{12–22} The work of Alivisatos et al., in which tetrapod structures of CdSe and

* Corresponding author. Tel.: 713-348-5650. Fax: 713-348-51. E-mail: whitmir@rice.edu.

[†] Department of Chemistry, Rice University.

[‡] Center for Biology and Environmental Nanotechnology, Rice University.

[§] Department of Chemical and Biomolecular Engineering, Rice University.

^{||} University of Houston.

[⊥] Department of Earth Science, Rice University.

- Burda, C.; Chen, X.; Narayanan, R.; El-Sayed, M. A. *Chem. Rev.* **2005**, *105*, 1025–1102.
- Yan, H.; He, R.; Pham, J.; Yang, P. *Adv. Mater.* **2003**, *15*, 402–405.
- Lee, S.-M.; Cho, S.-N.; Cheon, J. *Adv. Mater.* **2003**, *15*, 441–444.
- Cheon, J.; Kang, N.-J.; Lee, S.-M.; Lee, J.-H.; Yoon, J.-H.; Oh, S. J. *J. Am. Chem. Soc.* **2004**, *126*, 1950–1951.
- Hyeon, T.; Lee, S. S.; Park, J.; Chung, Y.; Na, H. B. *J. Am. Chem. Soc.* **2001**, *123*, 12798–12801.
- Sun, S.; Zeng, H. *J. Am. Chem. Soc.* **2002**, *124*, 8204–8205.
- Jun, Y.-w.; Casula, M. F.; Sim, J.-H.; Kim, S. Y.; Cheon, J.; Alivisatos, A. P. *J. Am. Chem. Soc.* **2003**, *125*, 15981–15985.

- Son, D. H.; Hughes, S. M.; Yin, Y.; Alivisatos, A. P. *Science* **2004**, *306*, 1009–1012.
- Hu, J.; Li, L.-s.; Yang, W.; Manna, L.; Wang, L.-w.; Alivisatos, A. P. *Science* **2001**, *292*, 2060–2063.
- Jin, R.; Cao, Y.; Mirkin, C. A.; Kelly, K. L.; Schatz, G. C.; Zheng, J. G. *Science* **2001**, *294*, 1901–1903.
- Tang, Z.; Kotov, N. A.; Giersig, M. *Science* **2002**, *297*, 237–240.
- Pan, Z. W.; Dai, Z. R.; Wang, Z. L. *Science* **2001**, *291*, 1947–1949.
- Ma, R.; Bando, Y.; Zhang, L.; Sasaki, T. *Adv. Mater.* **2004**, *16*, 918–922.
- McFadyen, P.; Matijevic, E. *J. Colloid Interface Sci.* **1973**, *44*, 95–106.
- Li, W.-J.; Shi, E.-W.; Zhong, W.-Z.; Yin, Z.-W. *J. Cryst. Growth* **1999**, *203*, 186–196.
- Chen, Z.-Z.; Shi, E.-W.; Zheng, Y.-Q.; Li, W.-J.; Xiao, B.; Zhuang, J.-Y. *J. Cryst. Growth* **2003**, *249*, 294–300.
- Wu, Z.; Shao, M.; Zhang, W.; Ni, Y. *J. Cryst. Growth* **2004**, *260*, 490–493.
- Zhang, X.; Xie, Y.; Xu, F.; Xu, D.; Liu, H. *Can. J. Chem.* **2004**, *82*, 1341–1345.
- Siegfried, M. J.; Choi, K.-S. *Angew. Chem., Int. Ed.* **2005**, *44*, 3218–3223.
- Dick, K. A.; Deppert, K.; Larsson, M. W.; Martensson, T.; Seifert, W.; Wallenberg, L. R.; Samuelson, L. *Nat. Mater.* **2004**, *3*, 380–384.
- Manna, L.; Milliron, D. J.; Meisel, A.; Scher, E. C.; Alivisatos, A. P. *Nat. Mater.* **2003**, *2*, 382–385.
- Milliron, D. J.; Hughes, S. M.; Cui, Y.; Manna, L.; Li, J.; Wang, L.-W.; Alivisatos, A. P. *Nature* **2004**, *430*, 190–195.

CdTe are obtained owing to the availability of the energetically similar face-centered cubic (fcc) zinc blende and hexagonal wurtzite morphologies,²¹ is particularly relevant to our findings detailed below.

In this paper we wish to report how a reaction system can be controlled to produce manganese oxide nanoparticles of novel forms. These results potentially have application to a wide variety of compositions and involve changing the solvent system by varying the relative amounts of carboxylic acid and organic amine in the presence or absence of water. These findings imply a complex growth mechanism in which the effective solvent acidity and viscosity coupled with the solubility properties of the metal oxide in question allow production of the unusual forms, apparently through the promotion of rough surface formation as will be discussed below. Manganese oxides are known to adopt porous, metastable forms in addition to nonporous manganese oxides with a perovskite structure.²³ To date most of the reported studies on manganese oxides deal mainly with conventional forms such as nanorods, nanosheets, nanowires, nanospheres, nanobelts, or nanocubes.^{24–29} While our work was in preparation, a communication reporting similar results to those we have found appeared in print.³⁰ That paper suggested that the growth of the branched nanostructures occurred via oriented attachment, but our findings show that these structures arise from a more complicated dissolution/growth mechanism. The evolution of the structures observed gives insight into the growth mechanism; in addition, details about controlling a wide variety of nanoparticle shapes over a diverse range of reaction conditions are reported here. This paper details a much larger range of reaction conditions leading to additional shapes not previously observed. Furthermore, the communication³⁰ misassigned some of the transmission electron microscopy (TEM) diffraction peaks that are systematically absent for these fcc lattices. The origin of the spots those authors assigned as $\langle 110 \rangle$ reflections are described in a separate paper, which convincingly demonstrates that such spots arise from the development of Mn_3O_4 within the MnO shaped nanoparticles. After this paper was reviewed, another short report of shaped MnO nanoparticles appeared.³¹ That paper presented barbell-shaped particles similar to the ones found here upon annealing of the structures (vide infra). Furthermore, manganese oxides have important catalytic and ion exchange properties that justify their study.²⁴

Experimental Section

All work was carried out using standard Schlenk techniques. All reagents were obtained from Aldrich Chemical Co.; tri-*n*-octylamine (TOA; 98%), oleic acid (OA; 90%), oleylamine (70%), stearic acid (95%), ethanol, and hexane were distilled using standard methods.³² Bases and acids were dried separately at 100 °C under vacuum for about 4 h. $\text{Mn}(\text{HCOO})_2$ was dried under vacuum (10^{-2} Torr) at about 110 °C for 4 h. For all reactions described, the initial color indicative of decomposition to nanoparticles was green. With careful exclusion of air and in the presence of water, the slurries remained green after cooling; however, exposure to air would result in conversion to a brownish red color. Note that MnO is found in nature as the green mineral manganosite. TEM study was carried out using JEOL 2000FX and JEOL 2010 microscopes that were equipped with energy-dispersive spectrometers and operated at 200 kV. Conventional and high-resolution TEM imaging, selected area electron diffraction (SAED) and energy-dispersive spectroscopy (EDS) methods have been used for analysis of manganese oxides. In cases where the crystals proved sensitive, evidently from heating by the electron beam, reduction of the intensity of the electron beam and/or limiting the exposure time was done to minimize their influence on the crystals. The EDS data indicated that the manganese oxides had a homogeneous distribution of manganese ions with no other elements present, and the electron diffraction data confirmed that no other phases were present other than MnO. Atomic force microscopy (AFM) measurements were carried out using a Nanoscope IV Multimode atomic force microscope from Veeco Metrology. Viscosity measurements were carried out using RDA III Rheometrics Instruments. All the tests were run with a 40 mm parallel plate fixture. The minimum torque transducer range is 2–500 g/cm, and the normal force range is 2–1500 g.

X-ray diffraction (XRD) for lattice parameter determination was performed at Rigaku/MSC on a Rigaku Ultima III at 40 kV and 44 mA with unfiltered Cu $K\alpha$ radiation ($\lambda = 1.5406 \text{ \AA}$) using cross beam optics (CBO) and a hermetically sealed, high-temperature sample chamber at 298 K under vacuum. To minimize air exposure, sample transfer from the inert atmosphere to the sample chamber occurred quickly (< 5 min). An initial diffractogram of the green slurry corresponds to the MnO nanocrystals, dispersed on a platinum pan with a $0.02^\circ 2\theta$ step size and $2.5 \text{ s}\cdot\text{step}^{-1}$ in continuous mode, and confirmed that the sample matched the International Centre for Diffraction Data (ICDD) powder diffraction file (PDF) database card PDF 77-2363 for cubic MnO (space group $Fm\bar{3}m$). Repeat analysis at a $0.002^\circ 2\theta$ step size and $4 \text{ s}\cdot\text{step}^{-1}$ for ~ 11 h on discretized regions centered on (111), (200), (220), (311), (222), and (400) using CBO calculated $a = 4.446(8)$ with a standard deviation (σ) = 0.0003 \AA . CBO was used to precisely determine the lattice constant independent of sample height, in contrast to traditional focused beam optics. The sample was verified to be green upon removal, qualitatively confirming stability during analysis. Close analysis of the baseline failed to reveal any minor reflections characteristic of a superlattice. The sample slurry, dispersed on a microscope slide, transformed from green to brown over the analysis duration. The color change was attributed to air exposure rather than X-ray degradation as based on prior experience.

Synthesis of Conventional Shapes. Small nanocubes (Figure 1, 30–35 nm) were synthesized by decomposing a mixture of $\text{Mn}(\text{HCOO})_2$ (3 mmol) in the presence of TOA (9 mmol) and OA (15 mmol). The mixture was heated to 340 °C for 5–10 min (time counted after the green phase is formed). Using a molar ratio acid/amine of $\sim 1:4$ and $\text{M}/\text{H}_2\text{O}$, ~ 8 equiv of water hexagons were

(23) Brock, S. L.; Duan, N.; Tian, Z. R.; Giraldo, O.; Zhou, H.; Suib, S. L. *Chem. Mater.* **1998**, *10*, 2619–2628.

(24) Post, J. E. *Proc. Natl. Acad. Sci. U.S.A.* **1999**, *96*, 3447–3454.

(25) Yin, M.; O'Brien, S. *J. Am. Chem. Soc.* **2003**, *125*, 10180–10181.

(26) Park, J.; Kang, E.; Bae, C. J.; Park, J.-G.; Noh, H.-J.; Kim, J.-Y.; Park, J.-H.; Park, H. M.; Hyeon, T. *J. Phys. Chem. B* **2004**, *108*, 13594–13598.

(27) Seo, W. S.; Jo, H. H.; Lee, K.; Kim, B.; Oh, S. J.; Park, J. T. *Angew. Chem., Int. Ed.* **2004**, *43*, 1115–1117.

(28) Tian, Z.-R.; Tong, W.; Wang, J.-Y.; Duan, N.-G.; Krishnan, V. V.; Suib, S. L. *Science* **1997**, *276*, 926–930.

(29) Shen, X.; Ding, Y.; Liu, J.; Laubernds, K.; Zenger, R. P.; Polverejan, M.; Son, Y.-C.; Aindow, M.; Suib, S. L. *Chem. Mater.* **2004**, *16*, 5327–5335.

(30) Zitoun, D.; Pinna, N.; Frolet, N.; Belin, C. *J. Am. Chem. Soc.* **2005**, *127*, 15034–15035.

(31) Zhong, X.; Xie, R.; Sun, L.; Lieberwirth, I.; Knoll, W. *J. Phys. Chem. B* **2006**, *110*, 2–4.

(32) Perrin, D. D.; Armarego, W. L. *Purification of Laboratory Chemicals*; Pergamon Press: New York, 1988.

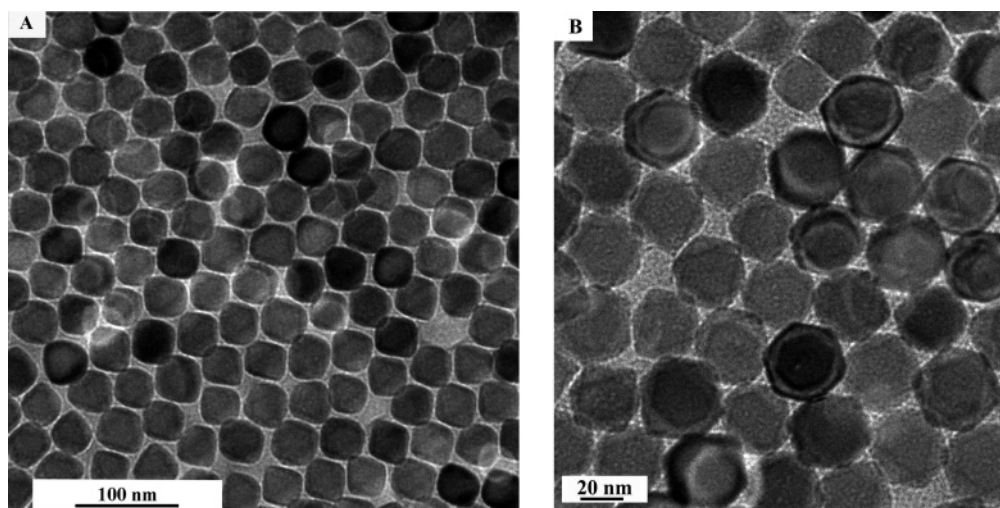


Figure 1. (A) MnO nanoparticles (35–40 nm) oriented with the {001} planes perpendicular to the electron beam. (B) MnO nanoparticles of 35–40 nm oriented with the {111} planes perpendicular to the electron beam.

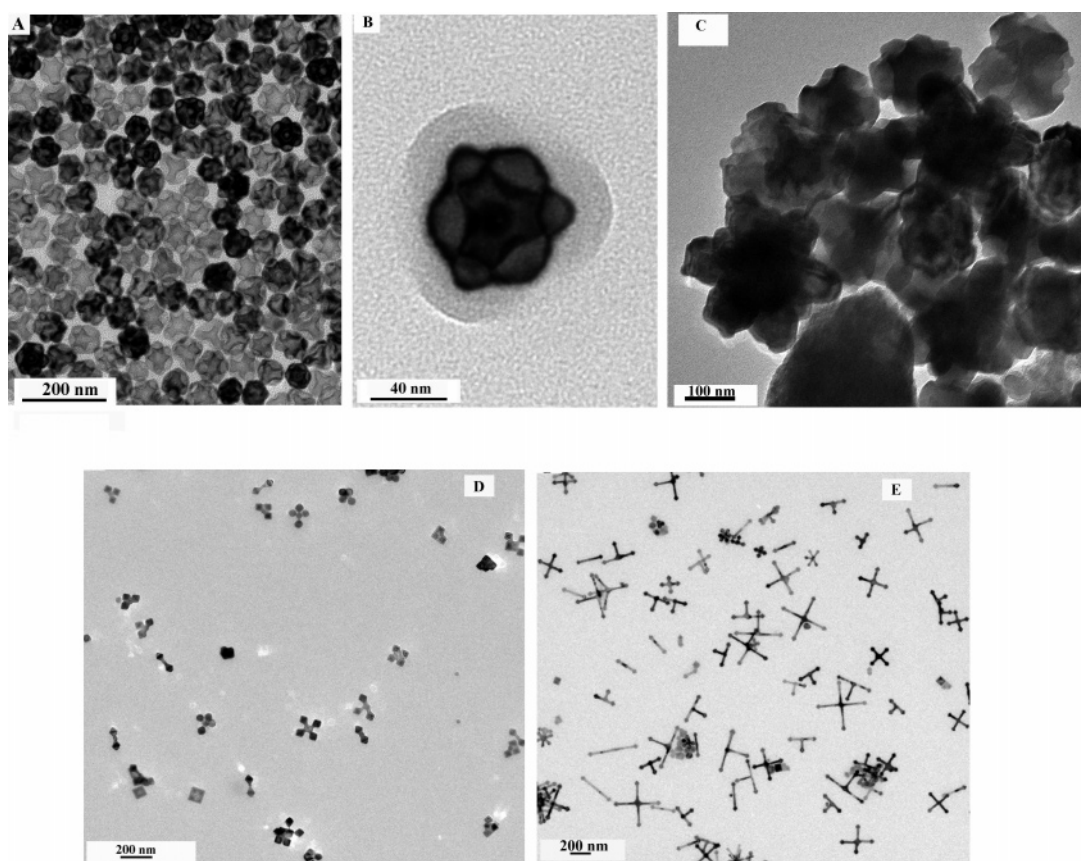


Figure 2. (A) Assembly of flower-shaped nanoparticle forms ($d = 56 \pm 5$ nm). (B) Expanded view of one flowerlike particle. (C) Star-shaped particles were observed after 1 h. (D) Nanocrosses (110–132 nm) and related shapes synthesized in the presence of TOA/OA (2:1) and $\text{H}_2\text{O}/\text{Mn}$ (4:1). (E) Nanohexapods with a large size distribution and their fragments synthesized in the presence of TOA/OA (2:1) $\text{H}_2\text{O}/\text{Mn}$ (~8:1).

formed (100–300 nm). Upon carrying out the decomposition in the presence of oleylamine (20 mmol) instead of TOA and OA smaller hexagonal shapes were also formed (35–40 nm; Figure 1). When OA is used alone no decomposition was observed at 340 °C; nevertheless, when pure stearic acid is used small cubic MnO particles (20 nm) were formed. Heating was accomplished using a standard heating mantle, and cooling was done by simple removal of the sample from the mantle.

Synthesis of Unusual Shapes. “Flower-Shaped” Particles. The synthesis of flower-shaped (Figure 2) particles requires that the TOA and OA be dried for 4 h under vacuum 10^{-2} Torr at 100 °C. The $\text{Mn}(\text{HCOO})_2$ was dried under vacuum 10^{-2} Torr at 110 °C, for 5

h, and kept in drybox. The synthesis was then carried out by decomposing a mixture of $\text{Mn}(\text{HCOO})_2$ (3 mmol) in the presence of TOA (14 mmol) and OA (6.34 mmol) to 340 °C for 5–10 min (time counted after the green phase is formed).

Nanocrosses. Nanocrosses (Figure 2) with dimensions of ~110 nm were synthesized by decomposing a mixture of $\text{Mn}(\text{HCOO})_2$ (3 mmol) in the presence of TOA (14 mmol) and OA (6.32 mmol). A controlled amount of water (4 equiv) relative to the metal salt concentration was added. The solution was annealed at ~340 °C for 5–10 min. The final product is a greenish solid that can be isolated by centrifugation and redispersed in hexane and tetrahydrofuran (THF). Upon oxidation the material turns brownish red.

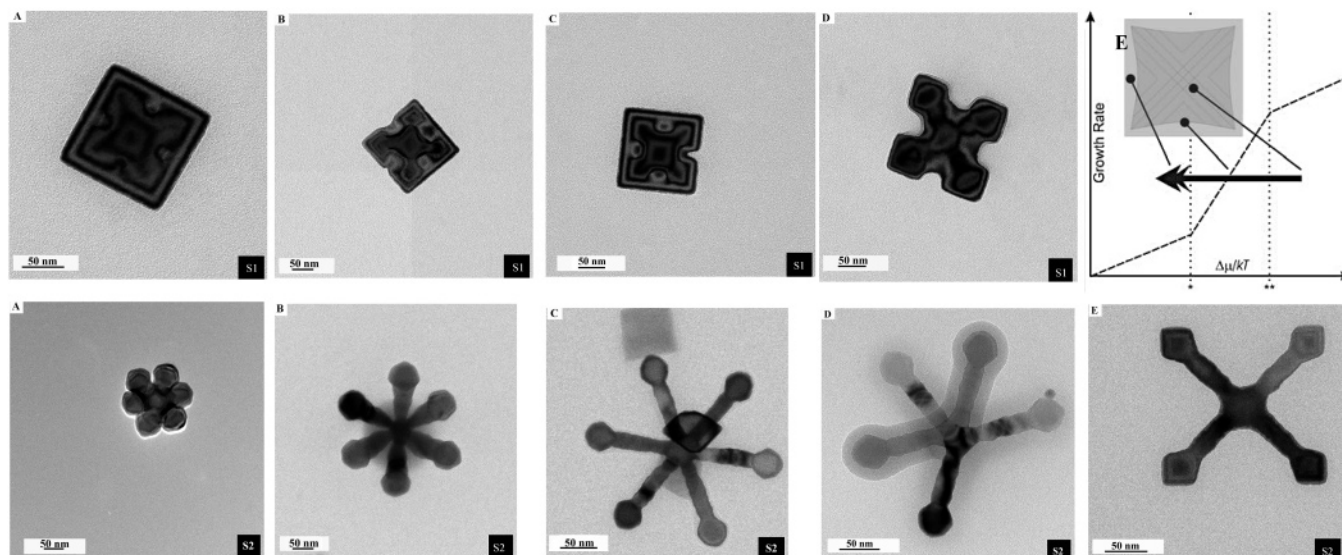


Figure 3. (Series 1) Progression of forms ranging from squares through partially “etched” (batch TOA/OA, 2:1; H₂O/Mn, ~4:1) squares (~132 nm) to fully formed cross forms and their derivatives. Part E (series 1) shows evolution of crystal growth conditions (arrow) and texture of the evolving nanocrystal. * and ** represent the limiting $\Delta\mu/kT$ values that distinguish spiral, nucleation, and dendritic growth fields (figure derived from the literature).³⁴ (Series 2) Progression of a hexapod nanoparticle to octahedral structures and derivatives thereof (batch TOA/OA, 2:1; H₂O/Mn, ~8:1).

Typical elemental analyses are as follows (Galbraith Analytical Laboratories): Mn, 66.23; C, 9.71; H, 1.69; N, <0.5%.

Octahedral Particles and Their Fragments. Hexapods and fragments thereof (Figure 2) with a dimension of ~150–300 nm were synthesized by decomposing a mixture of Mn(HCOO)₂·H₂O (3 mmol) in the presence of TOA (14 mmol) and OA (6.32 mmol). A controlled amount of water (H₂O/Mn, 1:4 molar ratio) was added so that the total water content was about ~8 mmol. The solution was annealed at ~340 °C for 5–10 min. The final product is a greenish solid that can be isolated by centrifugation and redispersed in hexane and THF. Upon oxidation the material turns brownish red. Typical elemental analyses of both nanocrosses and hexapods after precipitation in EtOH and drying under vacuum 10⁻² Torr leads to brownish powder that also analyzes as MnO.

Results and Discussion

Manganese(II) oxide nanoparticles can be conveniently grown by decomposing a Mn²⁺ carboxylate precursor in a heated mixture of OA and TOA. Tables 1–3 summarize a variety of conditions giving rise to different nanoparticle shapes. When the decomposition of Mn(HCOO)₂ (3 mmol) is carried out at 340 °C in acidic media (1:1, molar ratio) under anhydrous conditions, arrays of predominately square nanoparticles (35–40 nm; Figure 1A) are obtained that give diffraction patterns consistent with fcc MnO with {100} planes aligned perpendicular to the electron beam. These are similar in form to those previously reported by Yin and O’Brien,²⁵ which readily self-assemble. When the same decomposition is carried out at 250 °C in the presence of emulsified oleylamine (18 mmol, H₂O/Mn = 4:1) arrays of predominately hexagonal nanoparticles are formed instead that give diffraction patterns consistent with fcc MnO (Figure 1B) but oriented with the {111} planes perpendicular to the electron beam.

To understand why the nanocrystals adopt different preferential growth patterns, we further explored the range of reaction parameters and have discovered that highly unusual nanoscale forms can be obtained upon simple

modifications of the system. The ratio of carboxylic acid to amine is important, and the decomposition did not occur in the pure OA or TOA at 340 °C (in TOA, a slight green color appears as in the other decomposition reactions; however, the amount of nanoparticles produced is very small, and there was no evidence of nanocross formation) although decomposition in pure stearic acid produced 20–25 nm cubic-shaped particles. An increase in the relative amount of amine and the introduction of water (TOA/OA, 4:1; H₂O/Mn, 4:1) produced a mixture of predominately hexagonal forms along with a few additional cubic nanoparticles (100–150 nm).

When the reaction was performed in the presence of an excess of amine (TOA/OA, ~2:1), flowerlike nanoparticles (56 nm) were obtained (Figure 2A,B) with apparent six- or threefold symmetry representing the onset formation of small octahedra (vide infra). The star shapes appear sensitive to time, and upon extended annealing (~1 h), the particles grow in size and transform into more complicated star shapes (Figure 2C). Meanwhile, crystal faces begin to be less distinct.

Some of the most interesting forms (Figure 2D,E) were obtained reproducibly upon decomposition of Mn(HCOO)₂ (3 mmol) in TOA/OA (~2:1 molar ratio) with water present (typically 4:1 or 8:1 H₂O/Mn molar ratios). The various forms have clear relationships to each other and can be classified in two series. One series is based upon cross-shaped particles (Figure 3, series 1) which are on the order of 110–130 nm square. The other series involves a “bulky” octahedral parent structure leading to more compact octahedra and octahedral fragments (Figure 3, series 2). The images within each series can be viewed as interrelated as the cross-shaped nanocrystal morphology can also derive from an octahedral fragment with a pair of missing opposing arms; however, the nanocrosses can derive from the square plates with involvement of octahedral intermediates. In this regard, it is particularly intriguing that the nanocrystals in the first series contain a small number of square nanocrystals that have similar

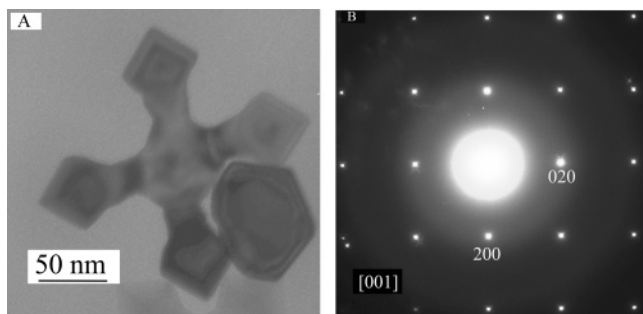


Figure 4. (A) Representative nanocross with (B) the corresponding SAED confirming the MnO fcc structure with $a = 0.44$ nm.

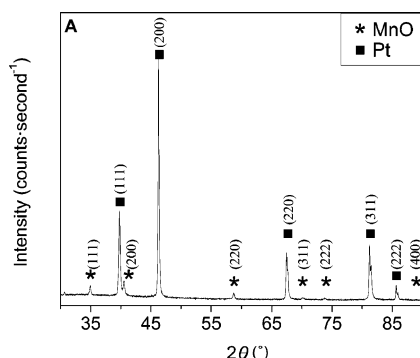


Figure 5. XRD analysis of MnO nanocrosses. (A) Structural characterization of MnO at Rigaku/MSC using CBO on a platinum (Pt) pan in an inert atmosphere at 298 K. The sample adopts space group $Fm\bar{3}m$ with $a = 4.446(8)$ Å.

dimensions as the nanocrosses and exhibit thickness extinction fringes (Figure 3A, series 1) in the TEM images that mimic the final form of the nanocrosses. The sequence in Figure 3, series 1, presents a characteristic progression in the crystal growth process with distinct changes in the kinetics and growth mechanism. The formation of channels as indicated by the TEM thickness fringes can be understood as a precursor to dendritic branch formation. This growth mechanism is discussed below in more detail in the context of crystal growth theory. Interestingly, an apparent self-assembled array in which cross-shaped motifs that resemble the ones found here are prominent has been reported.³³

Chemical composition of the nanocrosses was checked by EDS and confirmed to be pure manganese(II) oxide. No extra peaks from any impurities were found. Microstructural studies on fresh samples show extreme sensitivity to the electron beam, even when precautions were taken to minimize the beam influence on the structures. TEM diffraction studies confirm that the nanocrosses are crystalline and adopt a MnO fcc structure with lattice parameter $a = 0.44$ nm (Figure 4). The branches and the body of the crosses are of the same phase. This contrasts with the tetrapods of Alivisatos et al.²¹ that show a different crystal morphology of the core structure of the tetrapod compared to the branches. XRD analysis of the nanocrosses also confirmed their identity as fcc MnO (Figure 5).

To check the thermal stability of the particles we carried out in situ heating in the TEM on aged samples. These studies did not reveal any noticeable form or phase trans-

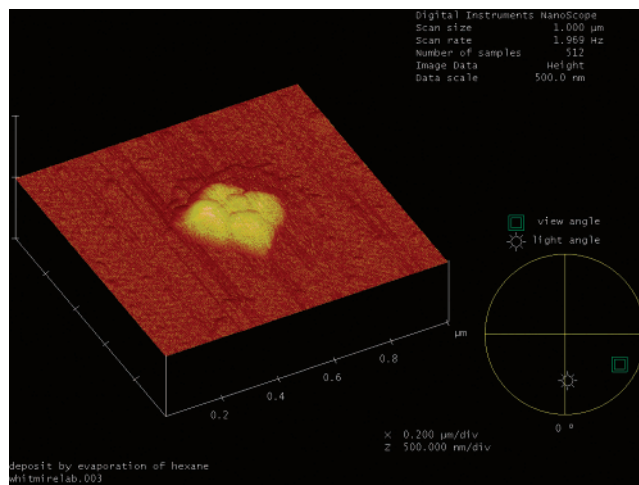


Figure 6. AFM image of an etched cube confirming the platelike nature of the nanocrosses. The crosses are approximately $300 \text{ nm} \times 300 \text{ nm}$ square with an average thickness of about 90 nm.

formations; however, weak amorphous diffraction rings were observed on the SAED patterns. This result led us to consider the possibility that the particles are more sensitive to electron beam damage when they are fresh. Upon exposing the fresh particles to an intense electron beam, dynamic phase and form transformations were observed in the electron beam. Details of these interesting phenomena will be reported separately.

To further shed light on the growth mechanism we probed the external morphology by imaging it along the lateral and frontal views, and the internal microstructure by high-resolution TEM and the chemical composition of the various regions of the crystals exhibiting thickness fringes were probed by EDS. No difference in structure or composition in the channel areas could be detected by TEM or EDS. AFM analysis of 50 nm crosses confirms that they are platelike (Figure 6).

Upon tilting the TEM stage, the three-dimensional structures of the nanoparticles were examined. The tilting data for the nanocrosses (not shown) was consistent with the AFM data (Figure 6) showing the platelike shape of those particles. The hexapods and related fragments (Figure 2E) were revealed to be based upon the octahedron (Figure 7). The complete octahedron is seen in Figure 7A–C while fragments of the octahedron are also observed including the five-vertex square-based pyramid (Figure 7E,F) and the four-vertex seesaw form (Figure 7G,H) in addition to the four-vertex cross, three-vertex T-forms, and two-pronged dumbbell forms (Figure 2). These forms can be named in accordance with the nomenclature adopted for polyhedral skeletal electron pair theory developed for cluster compounds where the succession of missing vertexes are named *closo*, *nido*, *arachno*, *hypho*, and so forth. Thus, the square pyramidal form is appropriately denoted as a *nido*-octahedron. The apparent hexagonal form in Figure 3A, series 2, was shown to be octahedral (trigonal antiprism) by dark field images where every other branch was found to be out-of-plane (Figure 7D).

To understand the origin of the cross-shaped particles, we carried out a systematic variation of experimental parameters.

(33) Soulantica, K.; Maisonnat, A.; Fromen, M.-C.; Casanove, M.-J.; Chaudret, B. *Angew. Chem., Int. Ed.* **2003**, *42*, 1945–1949.

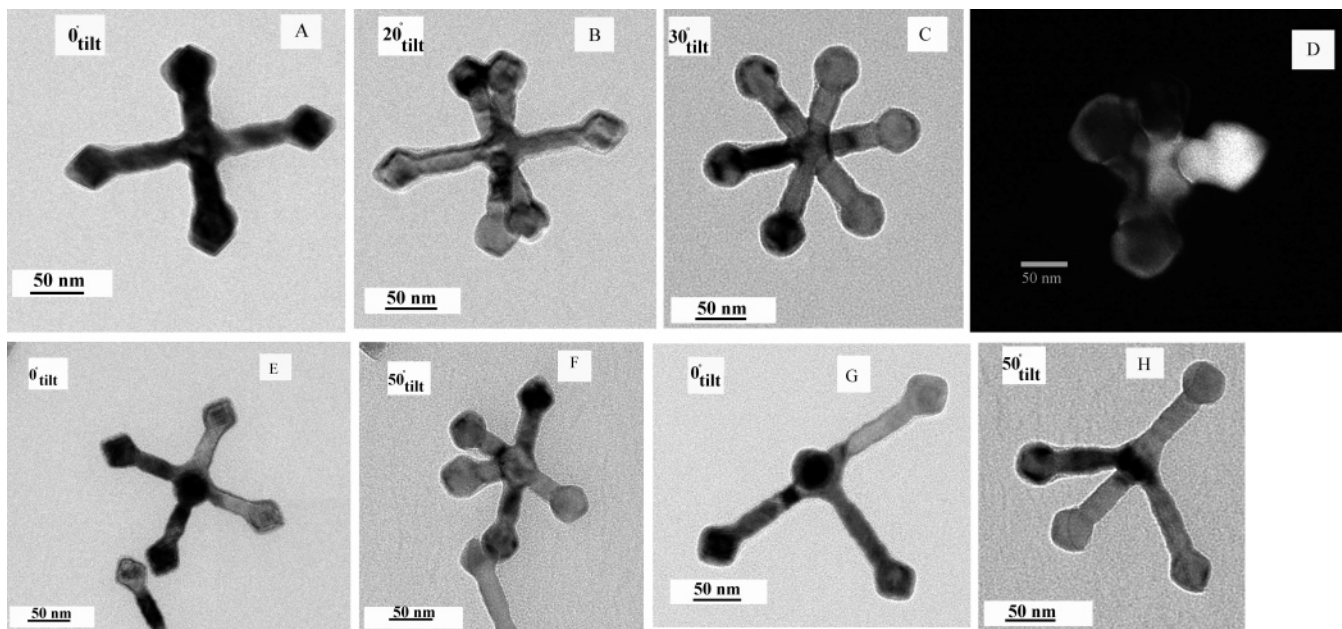
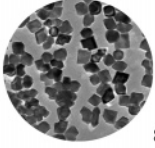
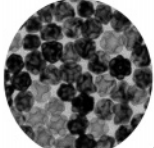
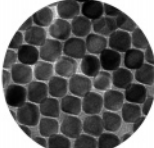
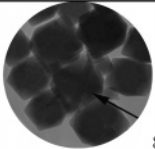
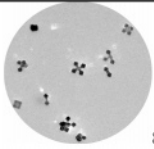
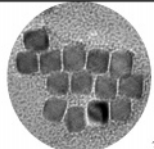
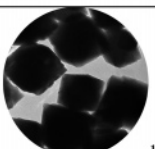
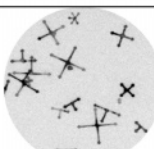
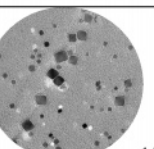


Figure 7. Nanohexapods and their fragments synthesized in the presence of TOA/OA (2:1) and $\text{H}_2\text{O}/\text{Mn}$ ($\sim 8:1$; A–C). (D) Dark field image of a hexapod showing its octahedral (trigonal antiprism) geometry where every other branch was found to be out of plane. Detail of the hexapod derivatives are obtained upon tilting each particle. (A, E) Transform upon tilting to octahedral (C) or square base pyramid (F); the tripod (G) transforms into trigonal base bipyramid (H).

Table 1. Summary of MnO Shaped Nanoparticles Grown at Various Reaction Conditions by Varying the Ratio of TOA/OA and the Ratio of $\text{H}_2\text{O}/\text{Mn}(\text{HCOO})_2$ ^a

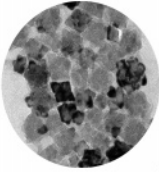
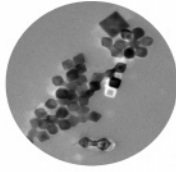
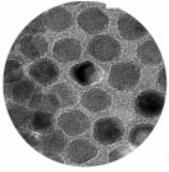
	TOA:OA ~ 4:1	TOA :OA ~2:1	TOA:OA~1:1
$\text{H}_2\text{O} : \text{Mn}(\text{HCOO})_2 = \sim 0$	 80–130nm	 56 nm	 35–40 nm
$\text{H}_2\text{O} : \text{Mn}(\text{HCOO})_2 = \sim 4:1$	 80–150 nm Some crosses from as well	 80–130 nm	 35–40 nm
$\text{H}_2\text{O} : \text{Mn}(\text{HCOO})_2 = \sim 8:1$	 150–300 nm	 150–300 nm	 biomodal

^a All syntheses were carried out by decomposing $\text{Mn}(\text{HCOO})_2$ (3 mmol) at 340–360 °C, for 5 ± 1 min (after the solution turns greenish). The rate of heating is 50 °C/min. The total concentration of surfactant is fixed at 8 mL, and the reaction is carried out in a 100 mL three neck flask.

The forms are sensitive to the concentration of water, acid–base ratio (Table 1), time (Table 2), and presence of air (Table 3). The ideal conditions (Figure 2C) for nanocross synthesis occur during the decomposition of $\text{Mn}(\text{HCOO})_2$ (3 mmol) under an inert atmosphere at a TOA/OA molar ratio of 2:1 (total volume = 8 mL) with a controlled amount of water ($\text{H}_2\text{O}/\text{Mn} = 4:1$) for 5 min (time counted from the start of the decomposition which is evidenced by a change of the color to green). Any deviation from these conditions

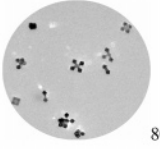
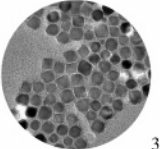
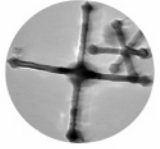
affects the shape. A moderate increase in water concentration favors the extension of the branches (Figure 2D). The particles generally appear thinner, more of them are linear (or barbell-shaped), and the ends of the branches tend toward spherical. In all cases, these forms are isolated as components of a green gel that is difficult to dry. Using more stringent drying conditions (10^{-2} Torr, $T = 250$ °C for 30 min) the form and morphology of the particles change to give even more compact branched and barbell-shaped particles.

Table 2. Summary of MnO Shaped Nanoparticles Grown for Various Lengths of Time^a

Time	time ≈ 1 min	time ≈ 5 min	time ≈ 1 h
<p>TOA :OA ~2:1</p> <p>H₂O :Mn(HCOO)₂ ≈ 4:1</p> <p>Result may change if one start from hydrous precursor</p>	 <p>80-130</p> <p>The particles are thin and surrounded by a stripe contrast</p>	 <p>100-132 nm</p>	 <p>12-15 nm</p>

^a Conditions are the same as those described in Table 1.

Table 3. Summary of MnO Shaped Nanoparticles Grown with Various Amounts of Air Added^a

Effect of air	Under argon	2cm ³ of air	Undefined traces of air
<p>TOA :OA ~2:1</p> <p>H₂O :Mn(HCOO)₂ ≈ 4:1</p> <p>(injected immediately before or after the change to green)</p>	 <p>80-130 nm</p>	 <p>35 nm</p>	<p>(final product highly viscous)</p>  <p>300-400nm/branch</p>

^a Other conditions are the same as those listed in Table 1.

As mentioned earlier, by varying the ratio of TOA/OA from 2:1 to ~4:1, regular cubic- or hexagonal-shaped particles were formed. The addition of water to the synthesis carried out in these conditions did not induce the shaping phenomena but led to an increase of size to (>110 nm) in agreement with previous observations in the literature.²⁷ These cubes or rhombohedra may show hexagonal shapes when observed along [111] and are often truncated and extremely beam sensitive because they show crystal dynamism and truncation concomitant with phase transformation under the TEM electron beam. In acidic media, only small crystallites (~35 nm) were obtained.

In the presence of air, the decomposition was variable and less reproducible. Small amounts of roughly shaped nanoparticles were more consistently obtained with moist air. However, when the process was performed with only traces of oxygen present (system purged using a weak vacuum of ~10⁻¹ Torr), crosses with extremely elongated branches (300–400 nm) were formed (see Table 3). The smallest crosses observed under the standard conditions are about 35 nm across. After adding a larger, controlled amount of air (2 cm³) to the solution immediately after the decomposition started (or immediately prior to it) only cubic-shaped particles of about 25–35 nm were formed. The investigation of the effect of time shows that in the typical conditions for nanocross synthesis (H₂O/Mn, ~4:1; TOA/OA, 2:1) regular forms are produced in the early stage of nucleation (<1 min) and then are etched (Figure 8).

At higher concentrations of water (H₂O/Mn, 8:1), the etching is observed at shorter time intervals. When the

hydrated manganese formate is used, the effect of water becomes pronounced and more easily reproduced. This may be due to better retention of water during the heating process.

Another interesting observation occurred upon interrupting the heating process after the first minute of the decomposition. When these solutions were cooled to room temperature and reheated for a further 5 min, nanorods mostly adopting barbell form, some with branches reminiscent of the nanocrosses, were obtained (Figure 9).

A key observation for the subsequent formation of unusual forms of the MnO nanocrystals discussed above is the formation of a negative curvature of the {110} planes (Figure 3, series 1) that leads to the formation of intermediate tunnels and ultimately to dendritic growth at the corners. Classical crystal growth theory offers a preliminary explanation to this problem. An important prerequisite for such an explanation is the presence of *rough* faces in the sense of crystal growth theory.³⁴ Results from our AFM study support this assumption (Figure 5), and high-resolution TEM images have shown that the faces are indeed rough. According to crystal growth theory, we can distinguish three different growth mechanisms: (1) spiral growth, (2) nucleation growth, and (3) dendritic growth. Kuroda et al.³⁵ have discussed the grain size dependence of the boundaries as a function of $\Delta\mu/kT$ with consideration of the Berg effect, in which a hopper morphology arises from fast crystal growth as a result of an

(34) Sunagawa, I. *Crystals Growth, Morphology and Perfection*; Cambridge University Press, 2005; p 295.

(35) Kuroda, T.; Irisawa, T.; Ookawa, A. *J. Cryst. Growth* **1977**, *42*, 41–46.

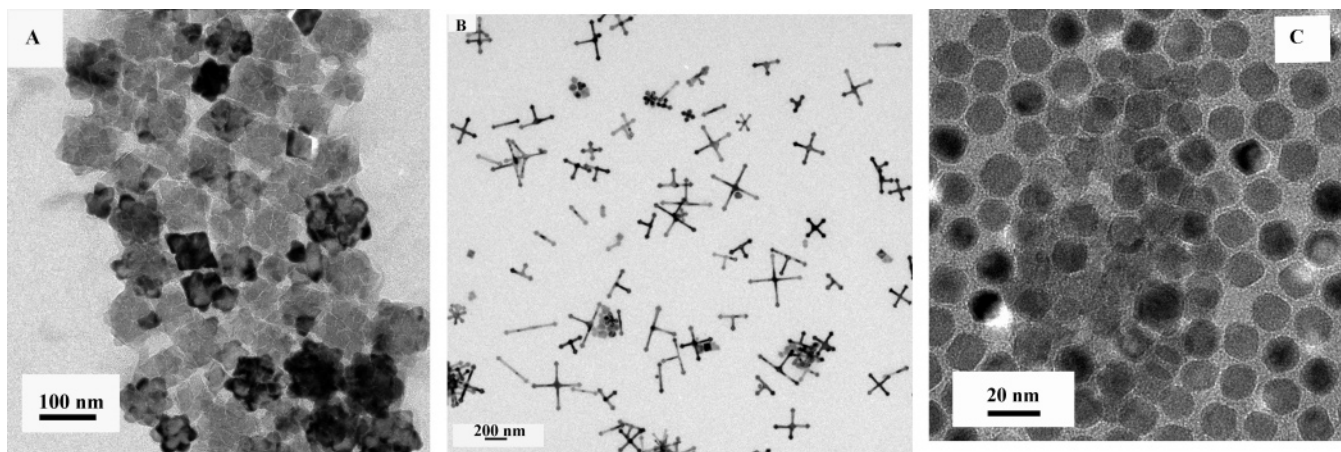


Figure 8. (A) Rhombohedral and pseudo-hexagonal shapes obtained after 1 min of growth. (B) Hexapods and derived fragments obtained when the reaction is carried out using the standard conditions but stopped after 5 min. (C) Self-assembled particles observed upon extending the time to 1 h.

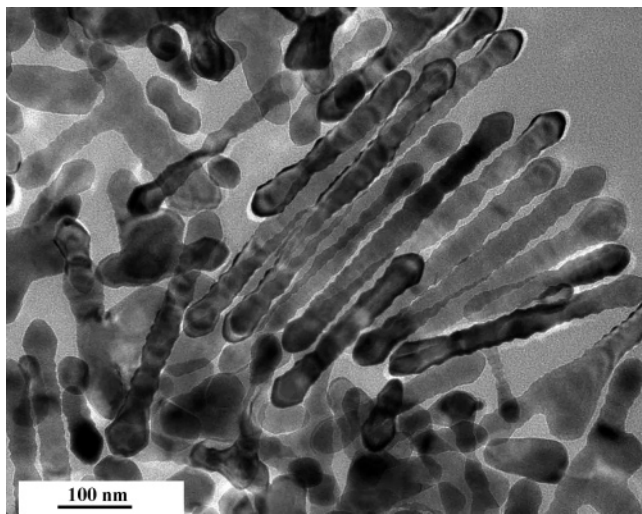


Figure 9. Barbell rods and tripods obtained starting from $\text{Mn}(\text{HCOO})_2 \cdot \text{H}_2\text{O}$ after cooling the solution for 1 min followed by reheating for 5 min.

increase in supersaturation in the vicinity of the growing crystal (see Figure 3E, series 1). A hopper morphology is one where a crystal and its branches form a continuous whole. As per Sunagawa,³⁴ we can summarize the following scenarios: a negatively curved, rough surface is formed if the growth kinetics are controlled by a nucleation mechanism (Figure 3E, series 1). This mechanism is driven by two-dimensional nucleation occurring mainly at the corners and edges. The resulting growth layers will advance toward the interior of the crystal face, leading to a so-called hopper crystal. In contrast, a spiral growth mechanism would result in a polyhedral crystal bounded by flat faces.

Studying the sequence of TEM images of Figure 3, series 1, we can interpret the evolution of the MnO crystals by analogy as a combination of these two growth mechanisms. We also have to consider an additional rapid, that is, dendritic, growth mechanism during the early stages of the crystallization process. The sketch of Figure 3E, series 1, demonstrates this development. After a rapid nucleation and dendritic growth phase, the mechanism changes to a two-dimensional nucleation mechanism that favors the Berg effect and leads consequently to the negative curvature of the $\{110\}$ planes. Further development into the spiral growth field is

responsible for the observed flat surfaces (Figure 3A, series 1). The resulting nanocrystal then contains an internal, negatively curved interface that resembles the channels seen in Figure 3A–C, series 1. Subsequently, these channels are opened up (Figure 3B,C, series 1), either by an etching process or by a return to the two-dimensional growth mechanism. A simple Gibbs–Thomson equation may describe this evolution as a function of the radius of curvature. The change from a flat (equilibrium) surface to a rough, negatively curved surface provides the driving force necessary for subsequent dendritic growth of the corners, ultimately leading to the observed nanocross forms. A detail that is not yet clear is whether the growth can occur via magic-sized clusters, which can be viewed as fragments of the bulk crystal lattice and which feed the growth of the crystal by Ostwald ripening, as has been proposed to explain the anisotropic growth of CdSe.³⁶

Our observations on the growth of the nanocrosses differs somewhat from the recent hypothesis for the growth of these particles which proposed growth by oriented attachment.³⁰ There is at least one mechanism that produces nanocrosses from plates rather than as octahedral fragments (cf. Figures 3 and 4). Furthermore, it is possible to obtain hexapods after only 5 min or even less using starting from hydrous $\text{Mn}(\text{HCOO})_2$. We conclude that the shape of the crosses is a result of solvothermal etching in conjunction with growth as described above in the frame of crystal growth from rough, negatively curved surfaces. The acidity of the solvent system seems to impact considerably the growth mechanism, thus ~ 80 – 300 nm rhombohedra or cubes form exclusively in a basic media and could be etched in the presence of a very weak concentration of carboxylic acid. Preliminary data indicate that the zigzag, herringbone-like contrast pattern is connected to oxidation of the MnO particles to Mn_3O_4 , a complex phenomenon that will be described in detail elsewhere. Other parameters such as time and concentration affects the growth as well. Standard cube shapes could be isolated in basic media at 5 min. These cubes or rhombohedra that exhibit regular patterns of thickness fringes may show rhombohedral or distorted hexagonal shapes when observed along $[111]$.

(36) Peng, X. *Adv. Mater.* **2003**, *15*, 459–463.

The decomposition almost certainly proceeds through an initial exchange reaction that leads to Mn(oleate)₂, which then decomposes at about 340 °C via vigorous explosions as observed by Hyeon et al.³⁷ The acid/base ratio coupled with the presence of water and/or oxygen at high temperatures is critical to the synthesis of the unusual form of nanoparticles of metal oxides. Organic amines have been used for etching purposes,³⁸ and OA, which forms manganese oleate,³⁷ has been used to digest oxides or oxo-hydroxy materials.³⁹ Water has been shown to promote restructuring of nanoparticles.⁴⁰ The coupled acid/base pair and the presence of water act in concert to produce a solvent system in which the nanoparticles grow under kinetically controlled conditions, and this may likely be influenced by the solvent viscosity, which has been implicated as an important factor in CdSe nanoparticle growth kinetics.⁴¹ The TOA/OA solvent system shows an interesting nonlinear change in viscosity as the mole fraction of the components is varied. There is a rise in viscosity in the solvent composition (measured at room temperature, measuring the viscosity at the reaction temperature was not possible) region near which the unusual forms of nanoparticles are created. This region of higher viscosity is also present in the presence of water, although the maximum viscosity occurs at a different solvent TOA/OA ratio. The presence of a controlled amount of water in a vapor phase and slight excess of carboxylic acid may accelerate the solvolysis of the growing oxide phase and thereby promote shaped growth. The solubility of the growing metal oxide and/or its related hydroxy and oxo/hydroxyl species in this medium would be crucial to the types of crystal surfaces formed and, therefore, the nanocrystal forms that are observed.

Conclusions

The morphogenesis of shaped MnO nanocrystals has been investigated and leads to a general approach to synthesize shaped crystals via a gel–sol process. Thus, in a mixture of carboxylic acid and organic base in the absence of water,

the thermal decomposition (~340 °C) of Mn(HCOO)₂ in acidic media lead to nonetched forms (square or hexagonal) with a small size (~35–40 nm), whereas in basic media nonetched bigger particles (80–300 nm, see Table 1) are obtained. The decomposition in the presence of traces of water and a slight excess of carboxylic acid leads to growth of more complex crystal forms, probably arising from increased solubility of the metal oxide (or hydroxide) in the vicinity of the growing crystal surface. In addition to the acid–base pair, other parameters such as time, temperature, and air appear critical. Most importantly, the internal substructure guides the growth and etching providing an elegant road map to the understanding of nanocrystal morphogenesis. This method, which is currently being extended to other oxides and quantum dots, promises to be general. For example, in the same solvent system iron oxide nanocrystals and lead sulfide nanocrystals are produced. These results will be reported separately. Further kinetic study of the growth using light scattering techniques will shed light on the mechanism and allow the establishment of a theoretical and predictive model.

The growth and shaping phenomena involved in the MnO nanocrystals seems to be dominated by a complex solvothermal growth/etching process occurring in conjunction with microstructural defects. As with other shaped nanocrystals, the unusual forms are produced by growth along the crystallographically preferred directions and these crystallographically preferred directions are dependent upon the local coordination environment of the ions involved. Thus the Alivisatos et al. tetrapods derive their tetrahedral shape from a core structure with a fcc arrangement of CdSe or CdTe, in which the Cd atoms are tetrahedrally coordinated and the hexapods observed here, which are also based upon an fcc lattice, have octahedrally coordinated Mn ions in a rock-salt like lattice, leading to forms derived from the octahedron. Thus we can expect other binary systems M_aX_b with different M/X ratios, different combinations of crystal lattice symmetries, and local coordination environments to produce other unique forms. Finally this approach will be further investigated to see whether natural self-assembly can emerge as a top-bottom decay of predefined geometries.

Acknowledgment. The authors would like to thank Rice University, the Robert Welch Foundation, and the Center for Biology and Environmental Nanotechnology for funding and Jason Hafner and Doug Natelson for fruitful discussions. Special thanks to Dr. Akhilesh Tripathi from Rigaku for assistance.

CM052492Q

- (37) Park, J.; An, K.; Hwang, Y.; Park, J.-G.; Noh, H.-J.; Kim, J.-Y.; Park, J.-H.; Hwang, N.-M.; Hyeon, T. *Nat. Mater.* **2004**, *3*, 891–895.
- (38) Li, R.; Lee, J.; Yang, B.; Horspool, D. N.; Aindow, M.; Papadimitrakopoulos, F. *J. Am. Chem. Soc.* **2005**, *127*, 2524–2532.
- (39) Yu, W. W.; Falkner, J. C.; Yavuz, C. T.; Colvin, V. L. *Chem. Commun.* **2004**, 2306–2307.
- (40) Zhang, H.; Gilbert, B.; Huang, F.; Banfield, J. F. *Nature* **2003**, *424*, 1025–1029.
- (41) Asokan, S.; Drujeger, K. M.; Alkhalid, A.; Carreon, A. R.; Mu, Z.; Colvin, V. L.; Mantzaris, N. V.; Wong, M. S. *Nanotechnology* **2005**, *16*, 2000–2011.